RESEARCH ARTICLE SUMMARY

PLANETARY SCIENCE

The atmosphere of Pluto as observed by New Horizons

G. Randall Gladstone,* S. Alan Stern, Kimberly Ennico, Catherine B. Olkin, Harold A. Weaver, Leslie A. Young, Michael E. Summers, Darrell F. Strobel, David P. Hinson, Joshua A. Kammer, Alex H. Parker, Andrew J. Steffl, Ivan R. Linscott, Joel Wm. Parker, Andrew F. Cheng, David C. Slater,† Maarten H. Versteeg, Thomas K. Greathouse, Kurt D. Retherford, Henry Throop, Nathaniel J. Cunningham, William W. Woods, Kelsi N. Singer, Constantine C. C. Tsang, Eric Schindhelm, Carey M. Lisse, Michael L. Wong, Yuk L. Yung, Xun Zhu, Werner Curdt, Panayotis Lavvas, Eliot F. Young, G. Leonard Tyler, the New Horizons Science Team

INTRODUCTION: For several decades, telescopic observations have shown that Pluto has a complex and intriguing atmosphere. But too little has been known to allow a complete understanding of its global structure and evolution. Major goals of the New Horizons mission included the characterization of the structure and composition of Pluto's atmosphere, as well as its escape rate, and to determine whether Charon has a measurable atmosphere.

RATIONALE: The New Horizons spacecraft included several instruments that observed Pluto's atmosphere, primarily (i) the Radio Experiment (REX) instrument, which produced near-surface pressure and temperature profiles; (ii) the Alice ultraviolet spectrograph, which gave information on atmospheric composition; and (iii) the Long Range Reconnaissance Imager (LORRI) and Multispectral Visible Imaging Camera (MVIC), which provided images of Pluto's hazes. Together, these instruments have provided data that allow an understanding of the current state of Pluto's atmosphere and its evolution.

RESULTS: The REX radio occultation determined Pluto's surface pressure and found a strong temperature inversion, both of which are generally consistent with atmospheric profiles retrieved from Earth-based stellar occultation measurements. The REX data showed near-symmetry between the structure at ingress and egress, as expected from sublimation driven dynamics, so horizontal winds are expected to be weak. The shallow near-surface boundary layer observed at ingress may arise directly from sublimation.

The Alice solar occultation showed absorption by methane and nitrogen and revealed the presence of the photochemical products acetylene and ethylene. The observed nitrogen opacity at high altitudes was lower than expected, which is consistent with a cold upper atmosphere. Such low temperatures imply an additional, but as yet unidentified, cooling agent.

A globally extensive haze extending to high altitudes, and with numerous embedded thin layers, is seen in the New Horizons images. The haze has a bluish color, suggesting a composition of very small particles. The observed scattering properties of the haze are consistent with a tholin-like composition. Buoyancy waves generated by winds flowing over orography can produce vertically propagating compression and rarefaction waves that may be related to the narrow haze layers.

Pluto's cold upper atmosphere means atmospheric escape must occur via slow thermal Jeans' escape. The inferred escape rate of nitrogen is ~10,000 times slower than predicted, whereas that of methane is about the same as predicted. The low nitrogen loss rate is consistent with an undetected Charon atmosphere but possibly inconsistent with sublimation/erosional features seen on Pluto's surface, so that past escape rates may have been much larger at times. Capture of escaping methane and photochemical products by Charon, and subsequent surface chemical reactions, may contribute to the reddish color of its north pole.

CONCLUSION: New Horizons observations have revolutionized our understanding of Pluto's atmosphere. The observations revealed major surprises, such as the unexpectedly cold upper atmosphere and the globally extensive haze layers. The cold upper atmosphere implies much lower escape rates of volatiles from Pluto than predicted and so has important implications for the volatile recycling and the long-term evolution of Pluto's atmosphere. ■

ON OUR WEB SITE

Read the full article at http://dx.doi.org/10.1126/science.aad8866

The list of author affiliations is available in the full article online.
*Corresponding author. E-mail: rgladstone@swri.edu
†Deceased.
Cite this article as G. R. Gladstone *et al.*, *Science* **351**, aad8866 (2016). DOI: 10.1126/science.aad8866

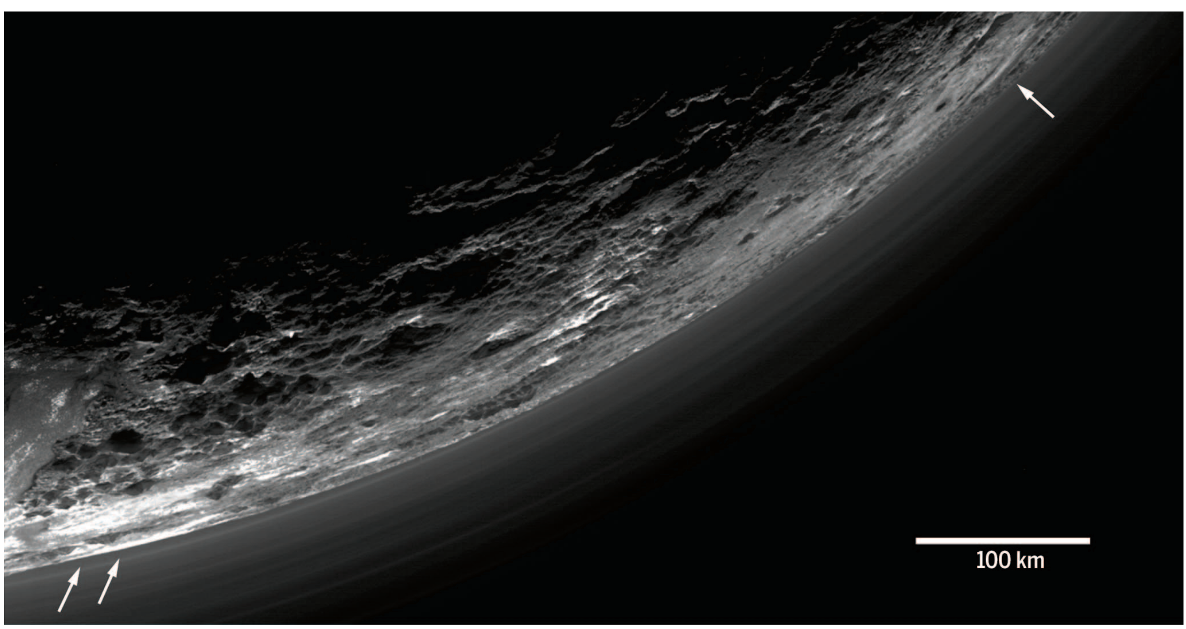

MVIC image of haze layers above Pluto's limb. About 20 haze layers are seen from a phase angle of 147°. The layers typically extend horizontally over hundreds of kilometers but are not exactly horizontal. For example, white arrows on the left indicate a layer ~5 km above the surface, which has descended to the surface at the right.

Downloaded from on March 17, 2016

RESEARCH ARTICLE

PLANETARY SCIENCE

The atmosphere of Pluto as observed by New Horizons

G. Randall Gladstone,[1,2]* S. Alan Stern,[3] Kimberly Ennico,[4] Catherine B. Olkin,[3] Harold A. Weaver,[5] Leslie A. Young,[3] Michael E. Summers,[6] Darrell F. Strobel,[7] David P. Hinson,[8] Joshua A. Kammer,[3] Alex H. Parker,[3] Andrew J. Steffl,[3] Ivan R. Linscott,[9] Joel Wm. Parker,[3] Andrew F. Cheng,[5] David C. Slater,[1]† Maarten H. Versteeg,[1] Thomas K. Greathouse,[1] Kurt D. Retherford,[1,2] Henry Throop,[7] Nathaniel J. Cunningham,[10] William W. Woods,[9] Kelsi N. Singer,[3] Constantine C. C. Tsang,[3] Eric Schindhelm,[3] Carey M. Lisse,[5] Michael L. Wong,[11] Yuk L. Yung,[11] Xun Zhu,[5] Werner Curdt,[12] Panayotis Lavvas,[13] Eliot F. Young,[3] G. Leonard Tyler,[9] the New Horizons Science Team‡

Observations made during the New Horizons flyby provide a detailed snapshot of the current state of Pluto's atmosphere. Whereas the lower atmosphere (at altitudes of less than 200 kilometers) is consistent with ground-based stellar occultations, the upper atmosphere is much colder and more compact than indicated by pre-encounter models. Molecular nitrogen (N_2) dominates the atmosphere (at altitudes of less than 1800 kilometers or so), whereas methane (CH_4), acetylene (C_2H_2), ethylene (C_2H_4), and ethane (C_2H_6) are abundant minor species and likely feed the production of an extensive haze that encompasses Pluto. The cold upper atmosphere shuts off the anticipated enhanced-Jeans, hydrodynamic-like escape of Pluto's atmosphere to space. It is unclear whether the current state of Pluto's atmosphere is representative of its average state—over seasonal or geologic time scales.

Major goals of the New Horizons mission were to explore and characterize the structure and composition of Pluto's atmosphere and to determine whether Charon has a measurable atmosphere of its own (*1*). Several instruments contribute to these goals, primarily (i) the Radio Experiment (REX) instrument (*2*), through uplink X-band radio occultations; (ii) the Alice instrument (*3*), through extreme- and far-ultraviolet solar occultations; and (iii) the Long Range Reconnaissance Imager (LORRI) and Multispectral Visible Imaging Camera (MVIC) (*4*, *5*), through high-phase-angle imaging. The associated data sets were obtained within a few hours of the closest approach of New Horizons to Pluto at 11:48 UT on 14 July 2015. Pressure and temperature profiles of the lower atmosphere are derived from the REX data, the composition and structure of the extended atmosphere are derived from the Alice data (supported by approach observations of reflected ultraviolet sunlight), and the distribution and properties of Pluto's hazes are derived from LORRI and MVIC images. This Research Article provides an overview of atmosphere science results.

A suggested atmosphere around Pluto (*6*–*11*) was confirmed by means of ground-based stellar occultation in 1988 (*12*, *13*) and subsequently studied with later occultations (*14*–*16*) and spectra at near-infrared and microwave wavelengths (*17*, *18*) and with models of increasing sophistication. These results revealed a primarily N_2 atmosphere with trace amounts of CH_4, CO, and HCN with complex surface interaction, an uncertain surface pressure of ~3 to 60 μbar, and a warm stratosphere at ~100 K above a much colder surface (38 to 55 K). On the eve of the New Horizons flyby, critical questions remained about the atmospheric temperature and pressure profiles, dynamics, the presence and nature of possible clouds or hazes, the escape of Pluto's atmosphere, and possible interactions with its large moon, Charon. The New Horizons flyby (*19*) enabled us to address these questions using radio occultations, ultraviolet occultations, and imaging at several phase angles between 15° and 165°.

Pressure and temperature

The New Horizons trajectory was designed to permit nearly simultaneous radio and solar occultations (*20*). The radio occultation was implemented in an uplink configuration by using 4.2-cm-wavelength signals transmitted by antennas of the NASA Deep Space Network and received by the REX instrument onboard New Horizons (*2*). The spacecraft passed almost diametrically behind Pluto as viewed from Earth, with ingress at sunset near the center of the anti-Charon hemisphere and egress at sunrise near the center of the Charon-facing hemisphere. Other characteristics of the REX observation are listed in table S1.

The location of Pluto's surface is indicated by a characteristic diffraction pattern in the REX

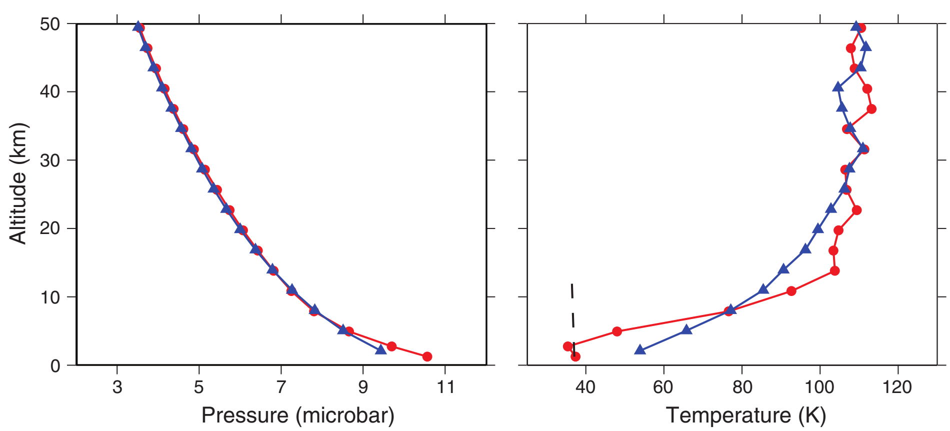

Fig. 1. Pressure and temperature in Pluto's lower atmosphere. (**Left**) Pressure. (**Right**) Temperature. These profiles were retrieved from radio occultation data recorded by the REX instrument onboard New Horizons. Diffraction effects were removed from the data (*53*), which greatly improves the accuracy of the results, and the conventional "Abel-transform" retrieval algorithm (*2*, *54*, *55*) was applied to the diffraction-corrected phase measurements. Each graph shows results at both entry (red line with circles) and exit (blue line with triangles), situated on opposite sides of Pluto. The profiles are most accurate at the surface, where the uncertainties in pressure and temperature are ~1 μbar and 3 K, respectively. Temperature fluctuations at altitudes of >20 km are caused by noise; no gravity waves were detected at the sensitivity of these measurements. The dashed line indicates the saturation temperature of N_2 (*29*).

[1]Southwest Research Institute, San Antonio, TX 78238, USA. [2]University of Texas at San Antonio, San Antonio, TX 78249, USA. [3]Southwest Research Institute, Boulder, CO 80302, USA. [4]National Aeronautics and Space Administration, Ames Research Center, Space Science Division, Moffett Field, CA 94035, USA. [5]The Johns Hopkins University Applied Physics Laboratory, Laurel, MD 20723, USA. [6]George Mason University, Fairfax, VA 22030, USA. [7]The Johns Hopkins University, Baltimore, MD 21218, USA. [8]Search for Extraterrestrial Intelligence Institute, Mountain View, CA 94043, USA. [9]Stanford University, Stanford, CA 94305, USA. [10]Nebraska Wesleyan University, Lincoln, NE 68504, USA. [11]California Institute of Technology, Pasadena, CA 91125, USA. [12]Max-Planck-Institut für Sonnensystemforschung, 37191 Katlenburg-Lindau, Germany. [13]Groupe de Spectroscopie Moléculaire et Atmosphérique, Université Reims Champagne-Ardenne, 51687 Reims, France.
***Corresponding author. E-mail: rgladstone@swri.edu**
†Deceased. ‡New Horizons Science Team authors and affiliations are listed in the supplementary materials.

amplitude measurements (2). According to scalar diffraction theory (21), the limb of Pluto is aligned with the location where the amplitude is reduced by 50% from its "free space" value, as determined from data recorded well before or well after the occultation by Pluto. (The change in amplitude from refractive bending in Pluto's atmosphere is negligible, in contrast to what occurs in stellar occultations observed from Earth.) At both entry and exit, the amplitude drops from 80 to 20% of its free-space value in a radial span of ~1.5 km. We used the solutions for the location of the surface at entry and exit to anchor the REX atmospheric profiles (Fig. 1), yielding an altitude scale with a relative uncertainty of ±~0.4 km.

The absolute radii at entry and exit are much less certain, owing to limitations on the accuracy of the reconstructed spacecraft trajectory. Because the occultation was nearly diametric, the main concern is with any systematic bias in the position of the spacecraft along its flight path. This sort of error causes an underestimate in the radius on one side of Pluto and an overestimate on the other side. However, the magnitude of the errors is nearly the same so that the mean radius is largely unaffected; its value is R_P = 1189.9 ± 0.4 km. This result is consistent with the global radius derived from images, 1187 ± 4 km (19). The difference, if real, could be a consequence of local topography or global flattening.

The atmospheric structure at altitudes of 0 to 50 km was retrieved from REX measurements of the Doppler-shifted frequency (or, equivalently, the phase) of the uplink radio signal (Fig. 1). We found that there is a strong temperature inversion at both ingress and egress for altitudes below ~20 km, which is qualitatively consistent with profiles retrieved from Earth-based stellar occultation measurements (16, 22, 23). However, there are two notable differences between the REX profiles at entry and exit, which indicate the presence of horizontal variations in temperature that had not been identified previously. First, the temperature inversion at entry is much stronger than its counterpart at exit; the derived mean vertical gradient in the lowest 10 km of the inversion is 6.4 ± 0.9 K km^{-1} at entry but only 3.4 ± 0.9 K km^{-1} at exit. Second, the temperature inversion at entry ends abruptly at an altitude of ~4 km, marking the top of a distinctive boundary layer. In contrast, the temperature inversion at exit appears to extend all the way to the surface, and we find no evidence for a boundary layer at that location. Because the radiative time constant of Pluto's atmosphere is 10 to 15 Earth years (24), equivalent to ~700 Pluto days, these differences in temperature structure cannot be attributed to nighttime radiative cooling or daytime solar heating within the atmosphere. A boundary layer had been discussed on energetic grounds or as a way to connect stellar occultation profiles to conditions at an unknown surface radius (23, 25–28). REX results indicate that the boundary layer is not uniform across Pluto.

We estimated the surface pressure through downward extrapolation of the REX pressure profiles (Fig. 1), obtaining values of 11 ± 1 μbar at entry and 10 ± 1 μbar at exit. Analysis of stellar occultation data from 2012 and 2013 has yielded essentially the same result, a pressure of 11 μbar at 1190 km radius (16). Hence, the mass of Pluto's atmosphere has not changed dramatically in recent years.

Downward extrapolation of the REX exit profile yields a temperature adjacent to the surface of 45 ± 3 K. For comparison, a surface covered in N_2 ice would have a temperature of 37.0 K to remain in vapor pressure equilibrium with the measured value of surface pressure (29). This may be indicative of a surface material less volatile than N_2 ice. Occultation exit was closer than entry to the subsolar latitude—52°N at the time of the observation—which would contribute to a warmer surface temperature in the absence of N_2 ice. [Where N_2 ice is present, any increase in insolation is balanced largely by latent heating, with only a small change in the ice temperature (30).]

At occultation entry, the mean temperature in the lowest 4 km above the surface is 37 ± 3 K, which is close to the saturation temperature of N_2 (29). This layer of cold air could arise directly from sublimation, and the close proximity of occultation entry to the region known informally as Sputnik Planum (SP)—with its large reservoirs of N_2, CO, and CH_4 ices (19, 31)—supports this interpretation. Moreover, Earth-based observations of Pluto imply that there is a strong zonal asymmetry in the distribution of N_2 ice (32); the abundance is largest near the REX entry longitude and smallest near the REX exit longitude. This raises the possibility that a scarcity of nearby sublimation sources could prevent the formation of a cold boundary layer at REX exit.

The cold boundary layer in the entry profile is steadily warmed by downward heat conduction in the overlying temperature inversion (33). We used a formula for the thermal conductivity of N_2 vapor (34) along with the measured temperature gradient to estimate the heating rate. The results indicate that it takes ~2 Earth years for this process to establish an inversion that extends to the ground. Without resupply of cold N_2, the boundary layer will vanish on this time scale. Hence, our interpretation implies that SP is an active sublimation source.

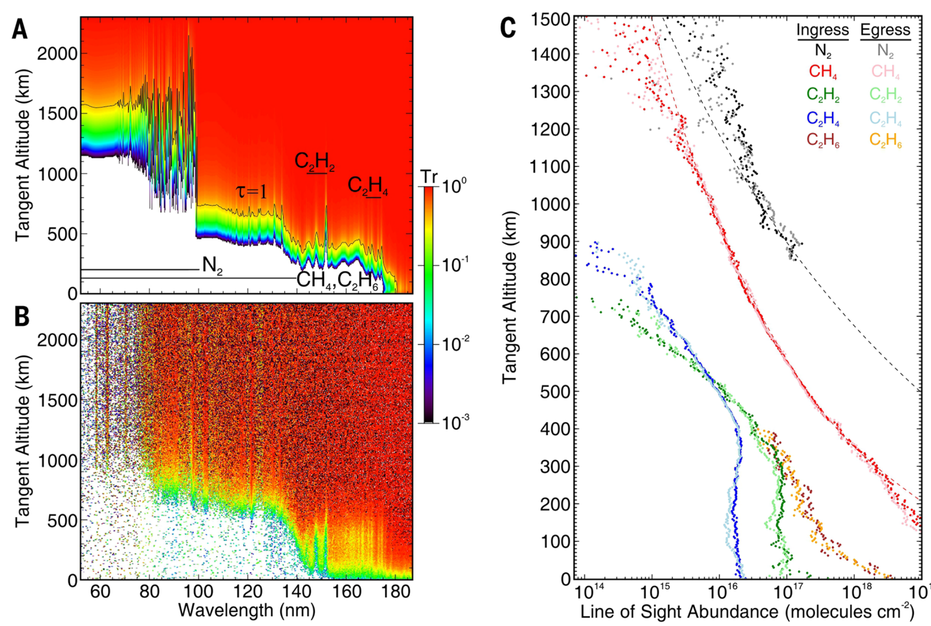

Fig. 2. Ultraviolet transmission of Pluto's atmosphere. (**A**) Line-of-sight (LOS) transmission as a function of ultraviolet wavelength and tangent altitude for the M2 model Pluto atmosphere (37), with the τ =1 line indicated along with the regions where N_2, CH_4, C_2H_2, C_2H_4, and C_2H_6 contribute to the opacity. N_2 absorbs in discrete bands for wavelengths 80 to 100 nm, with bands and an underlying continuum at wavelengths 65 to 80 nm and an ionization continuum at wavelengths of <65 nm. CH_4 dominates the opacity at wavelengths of <140 nm. C_2H_6 has a similar cross section to CH_4 but absorbs to 145 nm, where it contributes to the opacity. C_2H_2 has strong absorption bands at 144, 148, and 152 nm. C_2H_4 dominates the opacity at 155 to 175 nm. The model also contains C_4H_2, which accounts for much of the opacity at wavelengths 155 to 165 nm. (**B**) LOS transmission of Pluto's atmosphere determined from the Alice solar occultation data. The Alice data are normalized (at each ultraviolet wavelength) to unabsorbed levels at high altitude. In comparison with the model transmission, N_2 opacity begins at much lower altitudes (~500 km lower), whereas CH_4 opacity begins ~100 km higher than in the model. Pluto's atmosphere has somewhat less C_2H_2 and C_2H_4 than the model. Continuum absorption by Pluto's haze (not included in the model) is important at wavelengths >175 nm. (**C**) LOS column density profiles retrieved from the observed transmission data of (B) using known absorption cross sections for the indicated species. The quality of the data can be judged by the overlap of ingress and egress profiles (because the atmosphere is expected to be nearly spherically symmetric away from the surface) and by the amount of scatter in the data points. The dashed lines are LOS column densities computed by using the N_2 and CH_4 number density profiles in Fig. 3.

Last, the vertical resolution of the entry profile in Fig. 1 is not sufficient to determine the temperature lapse rate in the boundary layer. The results to date cannot distinguish an isothermal layer from one with a wet or dry adiabatic gradient.

Composition and chemistry

Models indicate that photochemistry in Pluto's upper atmosphere is similar to that of Titan and Triton (*35*–*38*). Methane (CH_4) is processed by far-ultraviolet sunlight into heavier hydrocarbons, and at Pluto's distance from the Sun, interplanetary hydrogen scattering of solar Lyman α photons provides a comparable secondary source of CH_4 photolysis, which is also effective at night and in winter (*39*). Extreme-ultraviolet sunlight photolyzes molecular nitrogen (N_2), leading to nitrile production in conjunction with CH_4 (*37*), and also ionizes N_2 to initiate the formation of large ions, which may lead to the production of high-altitude haze nuclei (*40*). Establishing Pluto's atmospheric composition as a function of altitude is important for understanding its atmospheric chemistry, and the solar occultations by the New Horizons Alice ultraviolet spectrograph (*3*) provide an excellent data set for this purpose. The circumstances of the solar occultations by Pluto and Charon are presented in tables S2 and S3, respectively. The transmission of Pluto's atmosphere is directly derived from the Alice ingress and egress data (Fig. 2; the full solar occultation light curve is presented in fig. S1). The transmission profile clearly indicates the altitude at which the tangent line-of-sight opacity reaches unity for a given wavelength and also provides a useful scale height at that level.

The Pluto solar occultation results are surprising in that the expected upper atmospheric opacity of N_2 at wavelengths ~65 to 100 nm is largely absent, and the opacity is mostly due to CH_4. At wavelengths longward of 100 nm, CH_4, C_2H_2, C_2H_4, C_2H_6, and haze account for a majority of the observed opacity. A model consistent with the observed transmission requires a much colder upper atmosphere than in pre-encounter models (Fig. 3). The absorption of sunlight in the 57- to 64-nm-wavelength range by N_2 at high altitudes (~850 to 1400 km) constrains the temperature of the upper atmosphere to be ~70 K. Such low temperatures are potentially achievable through cooling by C_2H_2 ν_5 band emission and HCN rotational line emission (if HCN is supersaturated, not in vapor pressure equilibrium at these cold temperatures). However, recent Earth-based observations by using the Atacama Large Millimeter/submillimeter Array (ALMA) suggest that the HCN abundances in Pluto's upper atmosphere are many times less than would be required (*16*, *18*). Currently, the details of exactly how Pluto's upper atmosphere is being cooled are poorly understood. Also, the ALMA data provide a definitive observation of CO on Pluto, which has not been detected in the Alice solar occultation data.

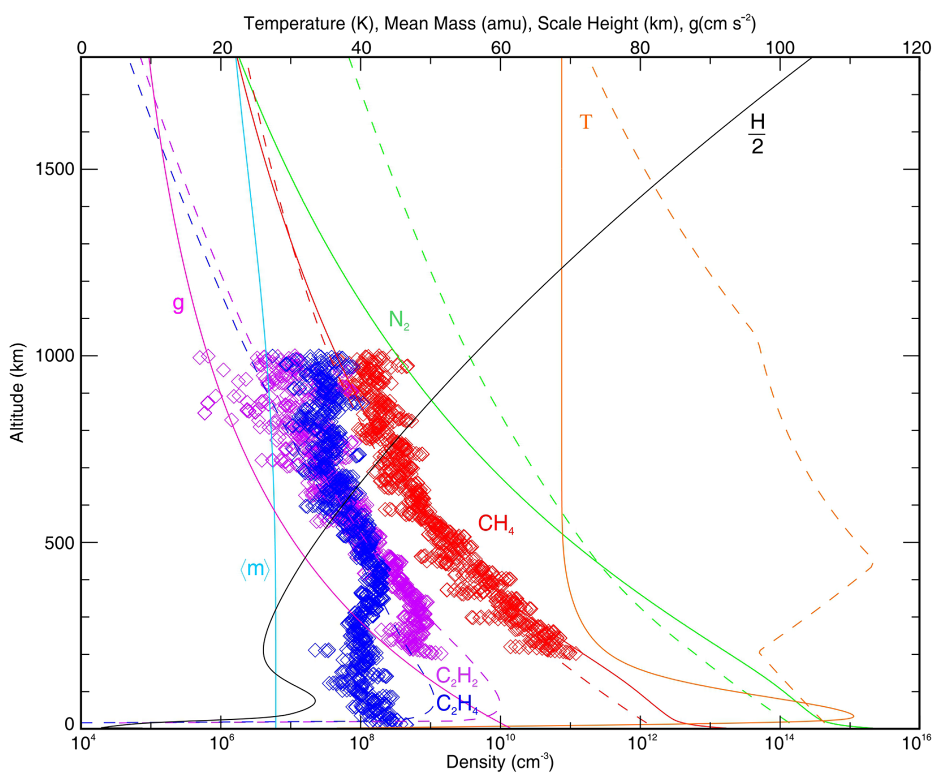

Fig. 3. Pluto's atmospheric composition and structure. Model profiles of temperatures, densities, and other relevant quantities (such as gravity *g*, mean mass ⟨*m*⟩, and N_2 density scale height *H*—plotted as *H*/2 in order to facilitate a common *x* axis range) in the atmosphere of Pluto are shown, which are consistent with the transmission results of Fig. 2. Methane, acetylene, and ethylene densities retrieved from the solar occultation data are indicated (diamonds). Pre-encounter model values (*37*) are given by dashed lines. Pluto's upper atmosphere is very cold (*T* ~ 70 K), resulting in a very low escape rate.

Hazes

Extensive, optically thin hazes are seen in New Horizons images of Pluto (Fig. 4), extending to altitudes of >200 km, with typical brightness scale heights of ~50 km. Distinct layers are present, which vary with altitude but are contiguous over distances of >1000 km. Separated by ~10 km, the layers merge, separate (divide into thinner layers), or appear and disappear when traced around the limb. Using radial brightness profiles at various points around the limb, prominent haze layers are found in LORRI images at altitudes of ~10, 30, 90, and 190 km, but in the highest-resolution MVIC images (<1 km/pixel), about 20 haze layers are resolved. The haze scale height decreases to ~30 km at altitudes of 100 to 200 km, which is consistent with the decreasing atmospheric scale height (Fig. 3). Although most obvious at high phase angles (Θ ~ 165° to 169°) with *I*/*F* values (observed intensity times π and divided by the incident solar flux) of ~0.2 to 0.3 at red wavelengths (in MVIC red, 540 to 700 nm, and LORRI images, 350 to 850 nm) and *I*/*F* values up to 0.7 to 0.8 at blue wavelengths (in MVIC blue images, 400 to 550 nm), the hazes are also seen at moderate scattering angles (for example, at *I*/*F* ~ 0.02 at Θ ~ 38°, in MVIC red and blue images) and are just barely detectable at low phase angles (for example, at *I*/*F* ~ 0.003 at Θ ~ 20°, in LORRI images) but are undetected at the lowest phase angles (Θ ~ 15°) on approach. Although the blue haze color is consistent with very small (radii *r* ~ 10 nm) particles (Rayleigh scatterers), their large high- to low-phase brightness ratio suggests much larger particles (with *r* > 0.1 μm); it is possible that they are aggregate particles (randomly shaped particles of a fraction of a micrometer in radius, composed of ~10-nm spheres), which could satisfy both of these constraints. The MVIC blue/red ratio increases with altitude, which is consistent with smaller particles at higher altitudes. As seen in Fig. 4, the haze is brightest just above the limb, and from this and other images, the haze is brightest around the limb near the direction of Pluto north.

Haze optical properties can be roughly estimated as a function of particle size by using Mie theory—for example, with optical constants of n = 1.69 and k = 0.018 (where n and k are the real and imaginary parts of the complex refractive index, respectively), which are appropriate for tholin-like particles (*41*) at the LORRI pivot wavelength of 607.6 nm (although over the LORRI bandpass, n varies between 1.63 and 1.72, whereas k varies between 0.11 and 0.0024). For optically thin conditions, $I/F \sim P(\Theta)\, \tau_{LOS}/4$, where P is the scattering phase function at phase angle Θ and τ_{LOS} is the line-of-sight opacity. On the basis of their large forward/backward scattering ratio, which is met by Mie-scattering particles with radii no smaller than ~0.2 μm, $P(165°) \sim 5$, leading to $\tau_{LOS} \sim 0.16$, or a vertical haze scattering optical depth of ~0.013. For particles of r ~ 0.2 μm, the scattering cross section of a single particle is

$\pi r^2 Q_S$ or ~3.4×10^{-9} cm^2 (with Q_S ~ 2.7 from Mie theory). Using $\tau \sim \pi r^2 Q_S n_{HAZE} H_{HAZE}$, where H_{HAZE} is the low-altitude haze scale height of 50 km, the haze density near Pluto's surface is n_{HAZE} ~ 0.8 particles/cm^3, or a column mass of 8×10^{-8} g cm^{-2} (assuming a particle density of 0.65 g cm^{-3}) (*42*).

If the haze particles are photochemically produced in a manner similar to Titan's hazes (*40*), an upper limit to their mass production rate is given by the photolysis loss rate of methane; from photochemical models (*37*, *38*), we estimate this at ~1×10^{-14} g cm^{-2} s^{-1}. In steady state, this is also the loss rate, so (dividing the column mass by the production rate) the haze residence time is calculated to be t_{HAZE} ~ 90 Earth days. By comparison, the time expected for 10-nm particles to settle through the lowest 10 km of the atmosphere is ~400 Earth days (fig. S2), whereas 0.2-µm particles would be expected to traverse this region much faster, in ~10 Earth days.

Dynamics

Pluto's atmospheric pressure and composition is buffered by sublimation equilibrium with surface ices (principally N_2, with minor amounts of CH_4 and CO ices). Solar-induced sublimation of these ices drives transport to colder surface regions. Subsequent condensation constrains pressure variations in the atmosphere above the first ½-scale height to $\Delta p/p < 0.002$ for a surface pressure ~10 µbar (*43*, *44*) and for ice $\Delta T/T < 0.002$ (*44*). For pressures <5 µbar, the radio occultation data exhibits global symmetry, as expected from sublimation-driven dynamics. Previously, ground-based stellar occultations also yielded symmetry within the error bars about the occultation midpoint (for example, as shown for the 2006 Siding Spring light curve) (*45*). With very little pressure variation in the current atmosphere on a global scale, horizontal winds are expected to be weak (no more than ~10 m s^{-1}). Radiative time constants (α_{RAD}) for Pluto's atmosphere above its planetary boundary layer are on the order of 10 to 15 Earth years (*24*), or α_{RAD} ~ 2.5×10^{-9} Hz. Diurnally driven dynamics with frequency of $\Omega = 2\pi/6.39$ days^{-1} = 1.14×10^{-5} Hz will be damped in amplitude by a factor ~$\alpha_{RAD}^2/(\alpha_{RAD}^2 + \Omega^2)$ ~ 5.6×10^{-8}. Although the surface likely has a short thermal response time constant, surface radiative exchange with the atmosphere is very weak, and the very steep positive temperature gradient in the near-surface layer as seen both in REX occultation data (Fig. 1) and ground-based stellar occultation data (*15*) should suppress convection and inhibit the formation of a deep global troposphere.

Gravity waves have previously been investigated as a source for scintillations seen in Earth-based stellar occultation data (*46*, *47*). Pluto's atmospheric dynamics can generate internal gravity (buoyancy) waves driven by sublimation forcing (*48*) and orographic forcing (wind blowing over topography). Mountains and mountain ranges with heights of 2 to 3 km have been detected with New Horizons imagery (*19*, *49*), and the distinct haze layers in Pluto's atmosphere are possibly a result of orographic forcing. For example, a

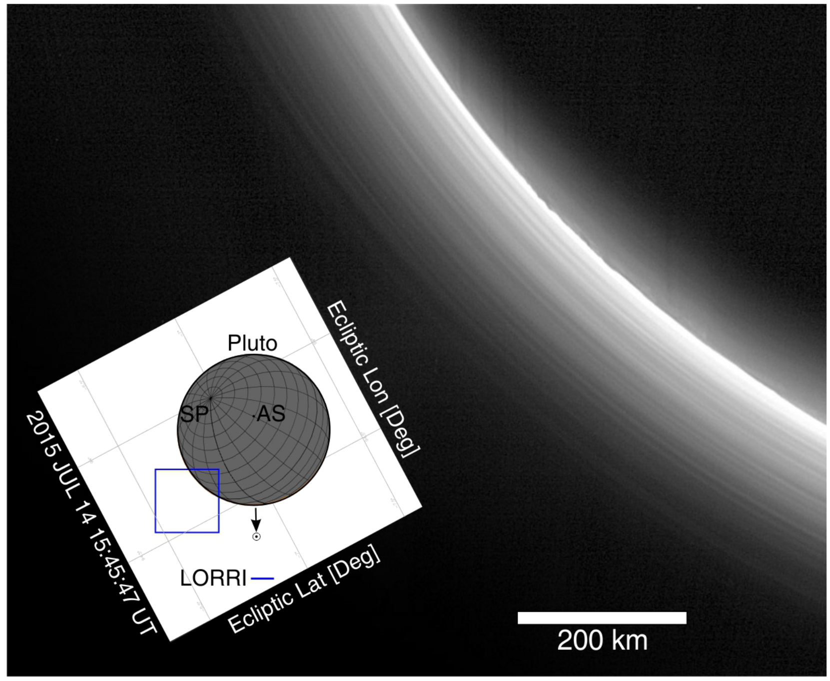

Fig. 4. Pluto hazes. LORRI two-image stack at 0.95 km pixel^{-1} resolution, showing many haze layers up to an altitude of ~200 km, as well as night-side surface illumination. Acquired on 14 July 2015 starting at 15:45:43 UTC (observation 5 of P_MULTI_DEP_LONG_1 at MET 299194661-299194671; 0.3 s total exposure time), at a range from Pluto of 196,586 km and a phase angle of 169°. The raw images have been background-subtracted and sharpened and have a square root stretch. (Inset) The orientation of the image, with Pluto's south pole (SP) indicated, along with the direction to the Sun (11° from Pluto), and the latitude and longitude of the sub–anti-Sun (AS) position.

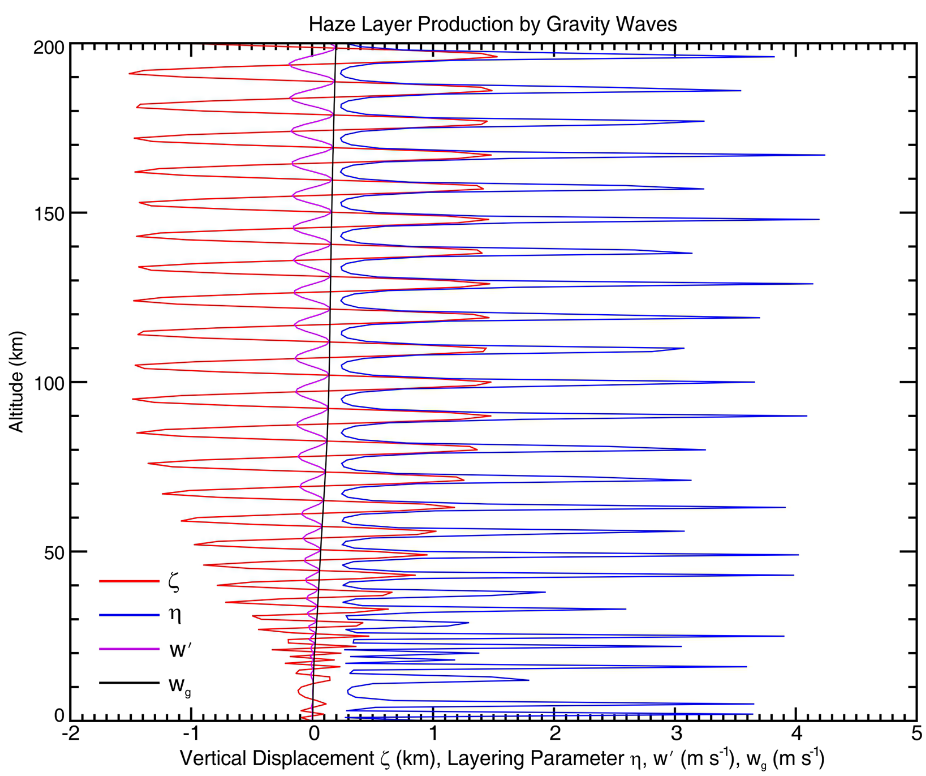

Fig. 5. Haze layer production. Haze particles undergo vertical displacements ζ by vertical gravity wave parcel velocity *w′*, which at saturation equals w_g, the vertical group velocity. Because *w′* is much larger than the sedimentation velocity, compression and rarefaction of haze particle densities are associated with gravity wave displacements. The quantity $\eta = (½\lambda_Z + 2\zeta)/(½\lambda_Z - 2\zeta)$ is a measure of compaction and layering.

u_0 = 1 m s^{-1} wind blowing over topography with height amplitude of h_0 = 1.5 km, horizontal wavelength λ_x ~ 120 km (zonal wavenumber $k_x = 2\pi/\lambda_x$ ~ $60/R_P$), meridional wavelength λ_y ~ 3600 km, and period $\tau = 2\pi/k_x u_0$ ~ 1.4 Earth days yields a vertical forcing velocity $w_0 \sim u_0 h_0 k_x$ ~ 0.08 m s^{-1}. Because of the small adiabatic lapse rate (~0.62 K km^{-1} at the surface and decreasing with altitude), the gravity wave reaches saturation amplitudes by an altitude of 10 km. Saturation occurs when the buoyancy-restoring force vanishes—when the sum of the wave and mean temperature gradients render the atmosphere adiabatic, and the vertical parcel velocity w' is equal to w_g, the vertical group velocity (*50*). At 10 km altitude, with any surface vertical forcing velocity w_0 > 0.008 m s^{-1}, the solution to the gravity wave equation yields saturated amplitudes for the wave temperature of T' ~ 0.7 K and for the vertical parcel velocity of w' ~ 0.01 m s^{-1} (with $w' = w_g$). These perturbation temperatures are consistent with the temperature profile, at the current level of analysis. The prime influence of horizontal winds, u, is on the vertical wavelength $\lambda_z \sim 2\pi u/N$, where N is the buoyancy frequency (~0.01 Hz at the surface and decreasing to ~0.001 Hz above 50 km), and the layering of the haze provides important constraints on this quantity. Shown in Fig. 5 is the vertical displacement, $\zeta = D^{-1}w' = w'/ik_x u$, of haze particles by gravity waves, with Lagrangian derivative D and $i = \sqrt{-1}$. Because w' is much larger than the sedimentation velocity (fig. S2), there is compression and rarefaction of haze particles associated with gravity wave displacements. If ½λ_z ~ 5 km and ζ ~ 1.5 km, compression leads to ~2 km separation and rarefaction to ~8 km separation between wave amplitude negative and positive peaks and could thus account for haze layering. Forcing by zonal winds would vanish at the poles, and variations of orography would affect the predictions as well, but gravity waves provide a viable mechanism for producing haze layers on Pluto.

Escape

Before the New Horizons flyby, the escape rate to space of N_2 from Pluto was expected (*33*) to be 0.7 × 10^{27} to 4 × 10^{27} molecules s^{-1}, with a preferred value of 2.8 × 10^{27} molecules s^{-1} based on estimates of Pluto's surface pressure and radius, as well as CH_4 and CO mixing ratios (*17*). This escape rate is fundamentally limited by solar extreme ultraviolet and far-ultraviolet net heating rates and by the effective area of Pluto's extended atmosphere. However, these pre-encounter calculations neglected cooling by photochemically produced HCN (*16*) and C_2H_2, which might reduce the net heating and hence the escape rate. On the basis of fits to the solar occultation transmission (Fig. 2), our calculated current escape rates of nitrogen and methane from Pluto's upper atmosphere are 1 × 10^{23} and 5 × 10^{25} molecules s^{-1}, respectively (with the exobase located at r ~ 2750 to 2850 km, where the N_2 and CH_4 densities are 4 × 10^6 to 7 × 10^6 cm^{-3} and 3 × 10^6 to 5 × 10^6 cm^{-3}, respectively). These are the Jeans escape rates—Pluto's atmosphere is not currently undergoing hydrodynamic escape—and they are low enough to strongly reduce the altitude of any interaction region between Pluto's upper atmosphere/ionosphere and the solar wind (*51*). If these rates are stable over a single Pluto orbit, the equivalent thickness of nitrogen and methane surface ice lost to space would be ~3 nm and 1.5 μm, respectively. If these rates were stable over the age of the solar system, the equivalent thickness of nitrogen and methane surface ice lost to space would be ~6 cm and 28 m, respectively. The relatively small amount of nitrogen loss is consistent with an undetected Charon atmosphere (of less than a pre-encounter prediction of ~8 pbar) (*52*) but appears to be inconsistent with the primarily erosional features seen on Pluto's surface (*49*), so that past N_2 escape rates may have occasionally been much larger. The loss of methane is much closer to predicted values (*37*), and a suggested origin for Charon's north polar red color (involving "varnishing" of the winter poles over millions of years through cold-trapping and polymerization of escaping hydrocarbons from Pluto) remains viable (*19*, *31*).

Conclusions

Observations made from New Horizons have already greatly altered our understanding of how Pluto's atmosphere works, even with many data remaining to be reduced and analyzed. LORRI, MVIC, and Linear Etalon Imaging Spectral Array (LEISA) imaging clearly reveal optically thin hazes extending to altitudes of at least 200 km. Photochemical models have long predicted the formation of higher hydrocarbons, and species such as acetylene (C_2H_2) and ethylene (C_2H_4) are clearly detected in the Alice solar occultation data (ultraviolet reflectance spectra also show the absorption signatures of C_2H_2 and C_2H_4). Last, the escape rate of Pluto's atmosphere is found to be much less than expected, although over time it may have left its signature on Charon (*19*, *31*).

Although most of the results obtained to date agree with each other, there are several problem areas: Is cooling by HCN self-limited because of condensation? Are the haze layers consistent with transport by winds? Does the escape of much more methane than nitrogen agree with geologic evidence? The data obtained by the New Horizons mission are likely to provide the answers and allow the development of a fully self-consistent description of Pluto's atmosphere.

REFERENCES AND NOTES

1. L. A. Young *et al*., New Horizons: Anticipated scientific investigations at the Pluto system. *Space Sci. Rev.* **140**, 93–127 (2008). doi: 10.1007/s11214-008-9462-9
2. G. L. Tyler *et al*., The New Horizons radio science experiment (REX). *Space Sci. Rev.* **140**, 217–259 (2008). doi: 10.1007/s11214-007-9302-3
3. S. A. Stern *et al*., Alice: The ultraviolet imaging spectrograph aboard the New Horizons Pluto-Kuiper Belt mission. *Space Sci. Rev.* **140**, 155–187 (2008). doi: 10.1007/s11214-008-9407-3
4. A. F. Cheng *et al*., Long-Range Reconnaissance Imager on New Horizons. *Space Sci. Rev.* **140**, 189–215 (2008). doi: 10.1007/s11214-007-9271-6
5. D. C. Reuter *et al*., Ralph: A Visible/Infrared Imager for the New Horizons Pluto/Kuiper Belt Mission. *Space Sci. Rev.* **140**, 129–154 (2008). doi: 10.1007/s11214-008-9375-7
6. M. H. Hart, A possible atmosphere for Pluto. *Icarus* **21**, 242–247 (1974). doi: 10.1016/0019-1035(74)90039-6
7. G. S. Golitsyn, A possible atmosphere on Pluto. *Sov. Astron. Lett.* **1**, 19 (1975).
8. D. P. Cruikshank, P. M. Silvaggio, The surface and atmosphere of Pluto. *Icarus* **41**, 96–102 (1980). doi: 10.1016/0019-1035(80)90162-1
9. U. Fink *et al*., Detection of a CH_4 atmosphere on Pluto. *Icarus* **44**, 62–71 (1980). doi: 10.1016/0019-1035(80)90055-X
10. L. Trafton, S. A. Stern, On the global distribution of Pluto's atmosphere. *Astrophys. J.* **267**, 872 (1983). doi: 10.1086/160921
11. N. Brosch, The 1985 stellar occultation by Pluto. *Mon. Not. R. Astron. Soc.* **276**, 571–578 (1995). doi: 10.1093/mnras/276.2.571
12. W. B. Hubbard, D. M. Hunten, S. W. Dieters, K. M. Hill, R. D. Watson, Occultation evidence for an atmosphere on Pluto. *Nature* **336**, 452–454 (1988). doi: 10.1038/336452a0
13. J. L. Elliot *et al*., Pluto's atmosphere. *Icarus* **77**, 148–170 (1989). doi: 10.1016/0019-1035(89)90014-6
14. A. S. Bosh *et al*., The state of Pluto's atmosphere in 2012-2013. *Icarus* **246**, 237–246 (2015). doi: 10.1016/j.icarus.2014.03.048
15. C. B. Olkin *et al*., Pluto's atmospheric structure from the July 2007 stellar occultation. *Icarus* **239**, 15–22 (2014). doi: 10.1016/j.icarus.2014.05.018
16. A. Dias-Oliveira *et al*., Pluto's atmosphere from stellar occultations in 2012 and 2013. *Astrophys. J.* **811**, 53 (2015). doi: 10.1088/0004-637X/811/1/53
17. E. Lellouch *et al*., Exploring the spatial, temporal, and vertical distribution of methane in Pluto's atmosphere. *Icarus* **246**, 268–278 (2015). doi: 10.1016/j.icarus.2014.03.027
18. E. Lellouch *et al*., (134340) Pluto. *IAU Circular* **9273**, 1 (2015).
19. S. A. Stern *et al*,. The Pluto system: Initial results from its exploration by New Horizons, *Science* **350**, aad1815 (2015).
20. Y. Guo, R. W. Farquhar, New Horizons mission design. *Space Sci. Rev.* **140**, 49–74 (2007). doi: 10.1007/s11214-007-9242-y
21. M. Born, E. Wolf, *Principles of Optics* (Cambridge Univ. Press, ed. 7, 1999).
22. B. Sicardy *et al*., Large changes in Pluto's atmosphere as revealed by recent stellar occultations. *Nature* **424**, 168–170 (2003). pmid: 12853950
23. J. L. Elliot *et al*., Changes in Pluto's atmosphere: 1988–2006. *Astron. J.* **134**, 1–13 (2007). doi: 10.1086/517998
24. D. F. Strobel, X. Zhu, M. E. Summers, M. H. Stevens, On the vertical thermal structure of Pluto's atmosphere. *Icarus* **120**, 266–289 (1996). doi: 10.1006/icar.1996.0050
25. J. A. Stansberry, J. L. Lunine, W. B. Hubbard, R. V. Yelle, D. M. Hunten, *Icarus* **111**, 503–513 (1994).
26. L. A. Young, "Bulk properties and atmospheric structure of Pluto and Charon," thesis, Massachusetts Institute of Technology, 1994.
27. E. F. Young *et al*., Vertical structure in Pluto's atmosphere from the 2006 June 12 stellar occultation. *Astron. J.* **136**, 1757–1769 (2008). doi: 10.1088/0004-6256/136/5/1757
28. E. Lellouch *et al*., Pluto's lower atmosphere structure and methane abundance from high-resolution spectroscopy and stellar occultations. *Astron. Astrophys.* **495**, L17–L21 (2009). doi: 10.1051/0004-6361/200911633
29. G. N. Brown Jr., W. T. Ziegler, Vapor pressure and heats of vaporization and sublimation of liquids and solids of interest in cryogenics below 1-atm pressure. *Adv. Cryog. Eng.* **25**, 662 (1980).
30. J. R. Spencer *et al*., "Volatile transport, seasonal cycles, and atmospheric dynamics on Pluto," in *Pluto and Charon*, S. A. Stern, D. J. Tholen, Eds. (Univ. of Arizona Press, 1997), pp. 435–473.
31. W. M. Grundy *et al*., Surface compositions across Pluto and Charon. *Science* **351**, aad9189-1 (2016).
32. W. M. Grundy, C. B. Olkin, L. A. Young, M. W. Buie, E. F. Young, Near-infrared spectral monitoring of Pluto's ices: Spatial distribution and secular evolution. *Icarus* **223**, 710–721 (2013). doi: 10.1016/j.icarus.2013.01.019
33. X. Zhu, D. F. Strobel, J. T. Erwin, The density and thermal structure of Pluto's atmosphere and associated escape processes and rates. *Icarus* **228**, 301–314 (2014). doi: 10.1016/j.icarus.2013.10.011
34. W. B. Hubbard, R. V. Yelle, J. I. Lunine, Nonisothermal Pluto atmosphere models. *Icarus* **84**, 1–11 (1990). doi: 10.1016/0019-1035(90)90154-2
35. M. E. Summers, D. F. Strobel, G. R. Gladstone, "Chemical models of Pluto's atmosphere," in *Pluto and Charon*, S. A. Stern, D. J. Tholen, Eds. (Univ. of Arizona Press, 1997), pp. 391–434.

36. L. M. Lara, W.-H. Ip, R. Rodrigo, Photochemical models of Pluto's atmosphere. *Icarus* **130**, 16–35 (1997). doi: 10.1006/icar.1997.5798
37. V. A. Krasnopolsky, D. P. Cruikshank, Photochemistry of Pluto's atmosphere and ionosphere near perihelion. *J. Geophys. Res.* **104** (E9), 21,979–21996 (1999). doi: 10.1029/1999JE001038
38. M. L. Wong, Y. L. Yung, G. R. Gladstone, Pluto's implications for a snowball Titan. *Icarus* **246**, 192–196 (2015). doi: 10.1016/j.icarus.2014.05.019
39. G. R. Gladstone, W. R. Pryor, S. A. Stern, Lyα@Pluto. *Icarus* **246**, 279 (2015). doi: 10.1016/j.icarus.2014.04.016
40. P. Lavvas *et al*., Aerosol growth in Titan's ionosphere. *Proc. Natl. Acad. Sci. U.S.A.* **110**, 2729–2734 (2013). doi: 10.1073/pnas.1217059110; pmid: 23382231
41. B. N. Khare *et al*., Optical constants of organic tholins produced in a simulated Titanian atmosphere—From soft x-ray to microwave frequencies. *Icarus* **60**, 127–137 (1984). doi: 10.1016/0019-1035(84)90142-8
42. S. M. Hörst, M. A. Tolbert, In situ measurements of the size and density of Titan aerosol analogs. *Astrophys. J.* **770**, L10 (2013). doi: 10.1088/2041-8205/770/1/L10
43. A. P. Ingersoll, M. E. Summers, S. G. Schlipf, Supersonic meteorology of Io—Sublimation-driven flow of SO_2. *Icarus* **64**, 375–390 (1985). doi: 10.1016/0019-1035(85)90062-4
44. L. A. Young, Volatile transport on inhomogeneous surfaces: I—Analytic expressions, with application to Pluto's day. *Icarus* **221**, 80–88 (2012). doi: 10.1016/j.icarus.2012.06.032
45. A. M. Zalucha, A. A. S. Gulbis, X. Zhu, D. F. Strobel, J. L. Elliot, An analysis of Pluto occultation light curves using an atmospheric radiative-conductive model. *Icarus* **211**, 804–818 (2011). doi: 10.1016/j.icarus.2010.08.018
46. M. J. Person *et al*., Waves in Pluto's upper atmosphere. *Astrophys. J.* **136**, 1510 (2008).
47. W. B. Hubbard *et al*., Buoyancy waves in Pluto's high atmosphere: Implications for stellar occultations. *Icarus* **204**, 284–289 (2009). doi: 10.1016/j.icarus.2009.06.022
48. A. D. Toigo, P. J. Gierasch, B. Sicardy, E. Lellouch, Thermal tides on Pluto. *Icarus* **208**, 402–411 (2010). doi: 10.1016/j.icarus.2010.01.027
49. J. M. Moore *et al*., The geology of Pluto and Charon through the eyes of New Horizons. *Science* **351**, 1284–1293 (2016).
50. D. C. Fritts, Gravity wave saturation in the middle atmosphere - A review of theory and observations. *Rev. Geophys. Space Phys.* **22**, 275 (1984). doi: 10.1029/RG022i003p00275
51. F. Bagenal *et al*., Pluto's interaction with its space environment: Solar wind, energetic particles, and dust. *Science* **351**, aad9045 (2016).
52. O. J. Tucker, R. E. Johnson, L. A. Young, Gas transfer in the Pluto-Charon system: A Charon atmosphere. *Icarus* **246**, 291–297 (2015). doi: 10.1016/j.icarus.2014.05.002
53. E. A. Marouf, G. L. Tyler, P. A. Rosen, Profiling Saturn's rings by radio occultation. *Icarus* **68**, 120–166 (1986). doi: 10.1016/0019-1035(86)90078-3
54. G. F. Lindal *et al*., The atmosphere of Titan—An analysis of the Voyager 1 radio occultation measurements. *Icarus* **53**, 348–363 (1983). doi: 10.1016/0019-1035(83)90155-0
55. D. P. Hinson, R. A. Simpson, J. D. Twicken, G. L. Tyler, F. M. Flasar, Initial results from radio occultation measurements with Mars Global Surveyor. *J. Geophys. Res.* **104** (E11), 26,997–27012 (1999). doi: 10.1029/1999JE001069

ACKNOWLEDGMENTS

We thank the NASA's New Horizons project for their excellent and long-term support. We thank our colleagues B. Bézard, J. Erwin, F. Forget, M. Gurwell, S. Gusewich, C. Hansen, A. Heays, K. L. Jessup, V. Krasnopolsky, E. Lellouch, B. Lewis, B. Sicardy, G. Stark, K. Stothoff, A. Toigo, R. Vervack, and R. Yelle for excellent advice, data, and useful comments. We thank the reviewers for their very useful comments. S.A.S. is also affiliated with Florida Space Institute, Uwingu, Golden Spike Co., and World View Enterprises. N.J.C. was a paid consultant to Southwest Research Institute. As contractually agreed to with NASA, fully calibrated New Horizons Pluto system data will be released via the NASA Planetary Data System at https://pds.nasa.gov in a series of stages in 2016 and 2017 owing to the time required to fully downlink and calibrate the data set.

SUPPLEMENTARY MATERIALS

www.sciencemag.org/content/351/6279/aad8866/suppl/DC1
Materials and Methods
Figs. S1 and S2
Tables S1 to S3
New Horizons Science Team Author List
References (*56*–*63*)

16 November 2015; accepted 17 February 2016
10.1126/science.aad8866